Non-Metal Redox Kinetics: Hypobromite and Hypoiodite Reactions with Cyanide and the Hydrolysis of Cyanogen Halides

Cynthia M. Gerritsen, Michael Gazda, and Dale W. Margerum*

Department of Chemistry, Purdue University, West Lafayette, Indiana 47907

Received June 3, 1993®

Pulsed-accelerated-flow spectroscopy is used to measure second-order rate constants (where the initial half-lives are 3–9 μs) for the reactions of cyanide ion with OBr^- and with OI^- (25.0 °C, μ = 1.00 M). The proposed mechanism includes parallel paths with halogen-cation transfer to CN^- by solvent-assisted reaction with OX^- (X = Br, I) and by direct reaction with HOX:

$$OX^- + CN^- + H_2O \xrightarrow{k_{ox}} XCN + 2OH^-$$

$$OX^- + H_2O \rightleftarrows HOX + OH^-$$

$$HOX + CN^- \xrightarrow{k_{HOX}} XCN + OH^-$$

The relative reactivities of the hypohalites with CN^- (k_{ox}) are as follows: OI^- (6×10^7 M^{-1} s^{-1}) ≈ OBr^- (5.7×10^7 M^{-1} s^{-1}) ≫ OCl^- (310 M^{-1} s^{-1}). The rate constants for the hypohalous acid reactions with CN^- (k_{HOX}) are as follows: HOBr (4.2×10^9 M^{-1} s^{-1}) > HOCl (1.22×10^9 M^{-1} s^{-1}). The base hydrolysis of ICN is studied spectrophotometrically by the appearance of I^- at 225 nm (ϵ = 12 070 M^{-1} cm^{-1}). Saturation kinetics are observed with increased OH^- concentration. This is attributed to rapid equilibration to give $HOICN^-$ (K_{OH} = 3.2 M^{-1}), which inhibits the OH^- attack at the carbon atom in ICN to form OCN^- ($k_4 = 1.34 \times 10^{-2}$ M^{-1} s^{-1}). The base hydrolysis of BrCN is studied by following the disappearance of the 105 amu peak with membrane introduction mass spectrometry. Rate constants for the reactions of BrCN with OH^- (k_{OH} = 0.53 ± 0.01 M^{-1} s^{-1}) and with CO_3^{2-} are determined (k_{CO_3} = (7.5 ± 0.3) × 10^{-3} M^{-1} s^{-1}). The relative reactivities of cyanogen halides for the base hydrolysis are as follows: ClCN ≫ BrCN ≫ ICN.

Introduction

Hypohalite ions react with cyanide ion in base to give the overall reaction in eq 1, where the halide ion and cyanate ion are products.

$$OX^- + CN^- \rightarrow X^- + OCN^- \quad (1)$$

These reactions might appear to be oxygen-atom transfer processes. However, it is well-known that halogens react with hydrocyanic acid to give cyanogen halides as products (eq 2).[1]

$$X_2 + HCN \rightarrow X^- + XCN + H^+ \quad (2)$$

The addition of chlorine or hypochlorite to waste water has long been an established process for the destruction of cyanide.[2] The reaction of HOCl and CN^- to give cyanogen chloride (eq 3)

$$HOCl + CN^- \rightarrow OH^- + ClCN \quad (3)$$

occurs even in basic solutions. In previous work[2] it was shown that CN^- reacts 4×10^6 times faster with HOCl than with OCl^-. As a result, very high hydroxide ion concentrations are needed to make the OCl^- path more favorable than the HOCl path. However, in high OH^- concentration the hydrolysis of ClCN (eq 4) is rapid and it is not possible to analyze for the initial products

$$ClCN + 2OH^- \rightarrow Cl^- + OCN^- + H_2O \quad (4)$$

to determine if the OCl^- path gives any ClCN or if OCl^- has reacted with CN^- to give OCN^- directly (eq 1).

In the present work we address three main questions: (1) Do hypohalites react with cyanide via O-atom transfer (eq 1), or do they proceed by X^+-transfer reactions (eq 5)? (2) What are the

$$H_2O + OX^- + CN^- \rightarrow 2OH^- + XCN \quad (5)$$

relative reactivities of OCl^-, OBr^-, and OI^- in their reactions with CN^-? (3) How rapidly do BrCN and ICN hydrolyze in base compared to ClCN?

Cyanogen bromide is the product of the reaction of hydrogen cyanide with bromine in acidic solution.[1] Nolan, Pendlebury, and Smith[3] studied the reaction in eq 6 under aqueous acidic

$$Br_2 + HCN \rightarrow BrCN + Br^- + H^+ \quad (6)$$

conditions at 25 °C, by the disappearance of Br_3^- at 267 nm where Br_3^- and Br_2 rapidly equilibrate. They established the rate law in eq 7, where k_a is 85 ± 5 M^{-1} s^{-1} and k_b is 5.7 ± 0.2

$$d[BrCN]/dt = -d[Br_2]_T/dt = (k_a + k_b/[H^+])[Br_2][HCN] \quad (7)$$

s^{-1}. Zhang and Field[4] studied the kinetics and mechanism of the BrO_3^- reaction with SCN^- in dilute $HClO_4$. They estimated a rate constant of 800 M^{-1} s^{-1} for eq 6 and a rate constant of 10 M^{-1} s^{-1} for the reaction between HOBr and HCN (eq 8).

* Abstract published in *Advance ACS Abstracts*, November 1, 1993.

(1) Williams, H. E. *Cyanogen Compounds; Their Chemistry, Detection, and Estimation*; Edward Arnold & Co.: London, 1948; pp 5–12.
(2) Gerritsen, C. M.; Margerum, D. W. *Inorg. Chem.* **1990**, *29*, 2757–2762.
(3) Nolan, M. F.; Pendlebury, J. N.; Smith, R. H. *Int. J. Chem. Kinet.* **1975**, *7*, 205–214.
(4) Zhang, Y. X.; Field, R. J. *J. Phys. Chem.* **1992**, *96*, 1224–1228.

0020-1669/93/1332-5739$04.00/0

However, these values were estimated from the study of a complicated oscillating chemical reaction system.

$$HOBr + HCN \rightarrow BrCN + H_2O \quad (8)$$

Smith[5] also studied the reaction of iodine with hydrogen cyanide (eq 9). At high pH, the reaction goes essentially to completion

$$I_2 + HCN \rightleftarrows ICN + I^- + H^+ \quad (9)$$

in the forward direction, whereas at low pH with excess iodide ion, the reverse reaction goes nearly to completion. Smith followed the disappearance of I_3^- at 353 nm under acidic conditions to determine the forward rate constant ($k_f = 65 \pm 2$ M^{-1} s^{-1}) and the reverse rate constant ($k_r = 39 \pm 1$ M^{-2} s^{-1}) for eq 9 at 25 °C.

As the reactions of hypobromous acid/hypobromite and hypoiodous acid/hypoiodite with CN^- are extremely rapid, pulsed-accelerated-flow (PAF) spectroscopy[6,7] is used in the present work to follow the disappearance of OBr^- or OI^- under second-order unequal concentration conditions. New methods to evaluate PAF data for very rapid second-order reactions are presented. Results from the second-order reactions with the pulsed-accelerated-flow spectrometer are included for initial half-lives as small as 3.1 μs.

Mass spectrometry, ^{13}C-NMR, stopped-flow, and UV–vis spectroscopy are used in the present work to identify the products (BrCN, ICN) and to examine their base hydrolysis.

Experimental Section

Reagents. All chemicals used were analytical grade. Stock solutions of sodium hydroxide were prepared by dilution of a saturated solution with distilled deionized water. The NaOH stock solution, which was protected from CO_2 contamination, was standardized by titration against potassium hydrogen phthalate with phenolphthalein indicator. The stock solution of sodium perchlorate was prepared from recrystallized $NaClO_4$ and was standardized gravimetrically. Buffer solutions were prepared from solid $NaHCO_3$ and Na_2CO_3, and pH was adjusted with NaOH or $HClO_4$. The OBr^- and OI^- solutions were prepared by adding Br_2 or I_2 to ice cold NaOH solutions (eq 10). The OBr^- was standardized

$$X_2 + 2OH^- \rightarrow OX^- + X^- + H_2O \quad (10)$$

spectrophotometrically at 329 nm ($\epsilon_{329} = 332$ M^{-1} cm^{-1})[8] and used within 2 h to prevent significant disproportionation.[9] Hypoiodite was standardized spectrophotometrically at 370 nm ($\epsilon_{370} = 60$ M^{-1} cm^{-1})[10] and used immediately after it reached 25 °C to minimize the effect of the relatively rapid disproportionation reactions of OI^-.[11,12] (Relevant wavelengths and corresponding molar absorptivities for the various species used in this study are given in Table I.) Solid NaCN was dissolved in NaOH solutions, and the CN^- concentration was determined by a potentiometric titration against silver nitrate using an Orion cyanide specific ion electrode with an Orion double junction reference electrode. Reactions were monitored by following the disappearance of either OBr^- at 329 nm or OI^- at 280 nm with the pulsed-accelerated-flow spectrophotometer.

The second-order PAF calibration reactions were performed by reacting $W(CN)_8^{4-}$ with $IrCl_6^{2-}$. The octacyano complex of tungsten was synthesized by the method of Leipolt et al.[13] The solid was stored in the dark to prevent photodecomposition prior to experiments. Acidic solutions were prepared by dissolving the solid in 0.5 M H_2SO_4 and by diluting quantitatively. Sodium hexachloroiridate(IV) hexahydrate ($Na_2IrCl_6 \cdot 6H_2O$) was used as received from Johnson Matthey Aesar. The concentration of $IrCl_6^{2-}$ was determined spectrophotometrically by its absorbance at 487 nm ($\epsilon_{487} = 4075$ M^{-1} cm^{-1}).[14] The reaction was monitored by following the disappearance of $IrCl_6^{2-}$ at 487 nm.

Cyanogen bromide was generated in solution from the reaction of bromine, hypobromous acid, or hypobromite with cyanide. Cyanogen iodide solutions were generated either by reaction of hypoiodious acid or hypoiodite with cyanide or was purchased from Aldrich Chemical Co.

UV–Vis Spectra. Kinetic data for the reaction of cyanogen iodide (25 °C, $\mu = 1.00$) were obtained with a Perkin-Elmer Lambda-9 spectrophotometer interfaced to a Zenith Data Systems Z-386/20. The reaction was monitored by the appearance of I^- (eq 11) at 225 nm ($\epsilon = 12\,070 \pm 100$ M^{-1} cm^{-1}). We determined the molar absorptivity by dilution of NaI solid with the addition of hydroxylamine to reduce traces of I_2 in solution that are invariably present due to O_2 oxidation. The ϵ value determined in this work for I^- is 16% smaller than a previously reported value[17] of 14 380 M^{-1} cm^{-1}. FitAll version 5.1, a nonlinear regression analysis program (MTR Software, Toronto, Canada), was used to determine the pseudo-first-order rate constants from the absorbance versus time data.

$$ICN + 2OH^- \rightarrow OCN^- + I^- + H_2O \quad (11)$$

Stopped-Flow Method. A Dionex-Durrum Model D-110 stopped-flow spectrophotometer (1.88-cm cell path) interfaced to a Zenith 151 PC with a MetraByte Dash-16 A/D converter was used to collect kinetic data. The formation of I^- from the reaction of IO^- with CN^- in high $[OH^-]$ was monitored at 225 nm, 25 °C, and $\mu = 1.0$ M.

Pulsed-Accelerated-Flow Method. Velocity-dependent absorbance changes were observed in the twin-path mixing/observation cell of the pulsed-accelerated-flow spectrophotometer, Model-IV (PAF-IV).[18] As the flow was linearly decelerated from 12.5 to 3.0 m s^{-1}, 250 measurements were taken. All solutions used for the PAF experiments were filtered and degassed. Solutions were placed in a water bath at 25.0 ± 0.1 °C for 20 min before data were collected. At least three PAF runs were averaged to obtain the experimental rate constant with its standard deviation.

To report the fast reactions measured by the PAF method under second-order conditions, an initial second-order half-life is used for comparison. The initial half-life is calculated from eq 12, where $(t_{1/2})_i$ is the initial half-life, C_A and C_B ($C_A > C_B$) are the initial concentrations of the two reactants (M), and k_{12} is the second-order rate constant (M^{-1} s^{-1}).

$$(t_{1/2})_i = \frac{1}{k_{12}} \frac{1}{(C_A - C_B)} \ln\left(\frac{2C_A - C_B}{C_A}\right) \quad (12)$$

^{13}C NMR Measurements. Enriched carbon-13 sodium cyanide (98.5 atom % ^{13}C), purchased from MSD Isotopes (lot no. 3353-p), was used for the NMR studies, and ^{13}C FT-NMR spectra were measured with a Varian Gemini-200 NMR spectrophotometer with a 5-mm broad-band probe at 50.289 MHz. The spectra were run in aqueous solution with at least 20% D_2O for signal lock and were proton decoupled by using the Waltz-16 decoupler method. A typical experiment used a 1-s acquisition time and a 3-s delay time, and 128 transients were collected over a period of 10 min. The pulse width was 10 μs, and the pulse angle, 41°. Each spectrum contained 30 000 data points for a 15 000-Hz window. ^{13}C FT-NMR spectral lines were referenced to an internal standard of dioxane (67.40 ppm).

Table I. Ultraviolet and Visible Absorption Spectral Characteristics

species	λ, nm	ε, M^{-1} cm^{-1}	ref
I^-	280	3.5	*a*
	260	32	*a*
	225	12070	*a*
OBr^-	329	332	*b*
OI^-	370	60	*c*
	280	190	*c*
	260	400	*c*

[a] This work. [b] Reference 8. [c] Reference 10.

(5) Smith, R. H. *Aust. J. Chem.* **1970**, *23*, 431–440.
(6) Nemeth, M. T.; Fogelman, K. D.; Ridley, T. Y.; Margerum, D. W. *Anal. Chem.* **1987**, *59*, 283–291.
(7) Jacobs, S. A.; Nemeth, M. T.; Kramer, G. W.; Ridley, T. Y.; Margerum, D. W. *Anal. Chem.* **1984**, *56*, 1058–1065.
(8) Troy, R. C.; Margerum, D. W. *Inorg. Chem.* **1991**, *30*, 3538–3543.
(9) Engel, P.; Opkatka, A.; Perlmutter-Hayman, B. *J. Am. Chem. Soc.* **1954**, *76*, 2010–2015.
(10) Paquette, J.; Ford, B. L. *Can. J. Chem.* **1985**, *63*, 2444–2448.
(11) Wren, J. C.; Paquette, S.; Sunder, S.; Ford, B. L. *Can. J. Chem.* **1986**, *64*, 2284–2296.
(12) Thomas, T. R.; Pence, D. T. *J. Inorg. Nucl. Chem.* **1980**, *42*, 193–196.
(13) Leipolt, J. G.; Bok, L. D. C.; Cilliers, P. J. *Z. Anorg. Allg. Chem.* **1974**, *407*, 350–352.
(14) Jorgenson, C. K. *Mol. Phys.* **1959**, *2*, 309–332.
(15) Farkas, L.; Lewin, M. *J. Am. Chem. Soc.* **1950**, *72*, 5766–5767.
(16) Shilov, E. *J. Am. Chem. Soc.* **1938**, *60*, 490–492.
(17) Awtrey, A. D.; Connick, R. E. *J. Am. Chem. Soc.* **1951**, *73*, 1842–1843.
(18) Bowers, C. P.; Fogelman, K. D.; Nagy, J. C.; Ridley, T. Y.; Wang, Y. L.; Evetts, S. W.; Margerum, D. W. To be submitted for publication.

Mass Spectrometry. Membrane introduction mass spectrometry (MIMS)[19] was used for product analysis and measurement of the base hydrolysis of BrCN. Mass spectra were obtained with a Finnigan TSQ 4500 triple quadrupole instrument equipped with an INCOS data system, where one quadrupole was used for mass analysis of the ions produced in the ion source, while the other two quadrupoles were operated in the RF only mode. Multiple ion detection (MID) was also employed. Ions were produced under 70-eV electron impact ionization conditions, and the source temperature was maintained at 190 °C while the manifold temperature was set at 120 °C.

A flat sheet of dimethylvinyl silicone polymer membrane (ASTM, VMQ Dow Corning) with a thickness of 0.005 in. was mounted in a specially constructed direct insertion probe,[20] which was inserted into the ion source of the mass spectrometer. Contact of the probe with the source block was made so that the membrane formed one of the walls of the heated ion source of the mass spectrometer.

Aqueous reactions of hypobromite, hypobromous acid, and bromide with cyanide were monitored using MIMS. The membrane probe was internally heated to 30 °C by a built-in heater operated by a programmable temperature controller. A peristaltic pump (Ismatic, Model 7618-30) was used to transport the solutions through the probe and across the membrane with a flow rate of 1 mL min^{-1}. Solutions were thermostated at 24 °C and were only in the probe for several seconds. The temperature upon exiting the probe was 26 °C. The reactants were mixed at the time the sample was introduced into the membrane probe; the initial signal detection was typically 11 s after introduction.

Results and Discussion

pK_a Determination for HOBr. The acid dissociation constant of HOBr was not known at 1.00 M ionic strength. A calibrated electrode was used to measure the change in $p[H^+]$ as $HClO_4$ was added to a basic OBr^- solution. The ionic strength was maintained at 1.00 M ($NaClO_4$), with the temperature thermostated at 25.0 ± 0.1 °C. The ratio of HOBr to OBr^- concentrations was calculated from the amount of $HClO_4$ added with a microburet, the initial concentration of OBr^-, the strong base end point, and the change in volume. The data were analyzed by use of eq 13 over the $p[H^+]$ range 9.3–8.3 with at least 30

$$pK_a = p[H^+] + \log \frac{[HOBr]}{[OBr^-]} \qquad (13)$$

points taken in each of two titrations. A pK_a value of 8.59 ± 0.03 (Table II) was found for $\mu = 1.00$ at 25.0 °C. This is in reasonable agreement with values reported at other ionic strengths. The pK_a value of 8.8 ± 0.1[8] at $\mu = 0.50$ was determined by the absorbance change at 300 nm for $[OBr^-]_T$ at various $p[H^+]$ values. Farkas and Lewin[15] found $pK_a = 8.7$ at 25 °C. Shilov[16] used electrochemical titration to determine a $pK_a = 8.7$ at 20 °C. The latter two studies did not specify the ionic strength or the precision of their values.

Calibration of PAF for Fast Second-Order Reactions. In previous PAF studies under second-order conditions,[6] an apparent rate constant, k_{12app} (M^{-1} s^{-1}), was measured as a function of the velocity, v, of the solutions in the observation tube. The value of k_{12app} was obtained by iteration on the value of R at different velocities from the absorbance data in eq 14.[21,22] The terms are defined as follows: M_{exptl} represents the fraction not reacted in the observation path, A_v is the absorbance at an individual velocity, b is the path length (1.025 cm), A_A is the absorbance of reactant A, A_B is the absorbance of reactant B, A_P is the absorbance of the products only, C_A is the initial concentration of reactant A, C_B is the initial concentration of reactant B, and q is the concentration ratio ($q = C_B/C_A$; $C_A > C_B$). A double-reciprocal

Table II. Comparison of Protonation Constants[a]

species	pK_a	ref
HOCl	7.47 ± 0.01	*b*
HOBr	8.59 ± 0.03	*c*
HOI	10.0 ± 0.3[d]	*e*
HCN	8.95	*f*

[a] Conditions: $\mu = 1.00$, and $T = 25.0 \pm 0.1$ °C. [b] Reference 2. [c] This work. [d] No ionic strength control. [e] Reference 11. [f] Reference 27.

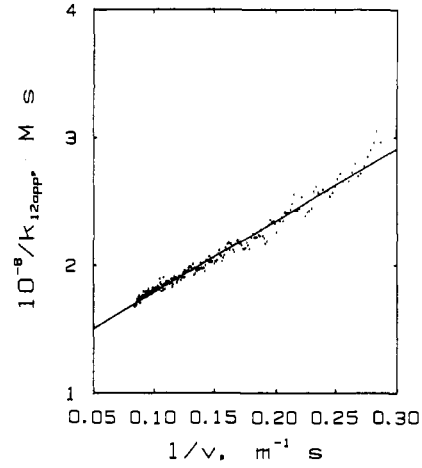

Figure 1. Double-reciprocal plot for the reaction of $W(CN)_8^{4-}$ + $IrCl_6^{2-}$ under second-order, unequal concentration conditions: initial $t_{1/2}$ = 57 μs. The plot is a least-squares line, weighted in proportion to velocity. The reciprocal of the intercept gives the experimental second-order rate constant of 0.87 ± 0.03 × 10^8 M^{-1} s^{-1}.

$$M_{exptl} = \frac{A_v - A_A(1-q) - A_P}{A_A + (1/q)(A_B - A_P)} = \frac{1-q}{R} \ln \frac{1 - qe^{-R}}{1-q} \qquad (14)$$

$$R = \frac{bk_{12app}C_A(1-q)}{v}$$

plot of $1/k_{12app}$ vs $1/v$ gave a slope that was inversely proportional to a mixing constant, k_{m12} (M^{-1} m^{-1}), and an intercept that was inversely proportional to the second-order rate constant, k_{12} (M^{-1} s^{-1}), according to eq 15.[6,23] This type of second-order double-

$$1/k_{12app} = 1/k_{m12}v + 1/k_{12} \qquad (15)$$

reciprocal plot has given reliable k_{12} values in previous studies,[6,23] where the initial half-life (defined by eq 12) was greater than 22 μs. However, this work shows that as the $(t_{1/2})_i$ value becomes smaller than 20 μs, serious deviations are observed when this technique is used with calibration reactions.

The redox reaction of Ir^{IV} and W^{IV} (eq 16) is used for the calibration reaction where the established rate constant[18] is (9.28

$$IrCl_6^{2-} + W(CN)_8^{4-} \rightarrow IrCl_6^{3-} + W(CN)_8^{3-} \qquad (16)$$

± 0.06) × 10^7 M^{-1} s^{-1}. At longer initial half-lives (>25 μs), the experimental rate constants agree within ±10% of the expected rate constant. Figure 1 is the second-order double-reciprocal analysis of the data for these conditions: $[IrCl_6^{2-}] = 1.58 \times 10^{-4}$ M, $[W(CN)_8^{4-}] = 1.78 \times 10^{-4}$ M. The experimental rate constant was found to be 8.7×10^7 M^{-1} s^{-1}, and $t_{1/2}$ is 57 μs, which is within 10% of the expected value. Other second-order calibration reactions with $(t_{1/2})_i$ from 29 to 118 μs (Table III) give reasonable results by using the double-reciprocal method. For eight sets of conditions, the average k_{12} by the double-reciprocal method is (9.2 ± 0.7) × 10^7 M^{-1} s^{-1}, where $(t_{1/2})_i$ is 29 μs or larger. Because the k_{12} value is obtained from the reciprocal of the intercept, the

(19) Kotiaho, T.; Lauritsen, F. R.; Choudhury, T. K.; Cooks, R. G.; Tsao, G. T. *Anal. Chem.* **1991**, *63*, 875A.
(20) Bier, M. E.; Kotiaho, T.; Cooks, R. G. *Anal. Chim. Acta* **1990**, *231*, 175–190.
(21) Gerischer, H.; Heim, W. *Z. Phys. Chem. (Munich)* **1965**, *46*, 345–352.
(22) Gerischer, H.; Heim, W. *Ber. Bunsen-Ges. Phys. Chem.* **1967**, *71*, 1040–1046.
(23) Vassilator, G.; Toor, H. L. *AIChE J.* **1965**, *11*, 666–672.

Table III. Comparison of the Second-Order Double-Reciprocal Plot, the Second-Order *M*-plot, and the Expanded Second-Order *M*-plot for the Calibration Data Collected by the Pulsed-Accelerated-Flow Method[a]

$10^4[IrCl_6^{2-}]$, M	$10^4[W(CN)_8^{4-}]$, M	ΔA_T	$t_{1/2}$,[b] μs	double reciprocal[c] $10^{-8}k_{12}$, M^{-1} s^{-1}	qe^{-R}	*M*-plot[d] $10^{-8}k_{12}$, M^{-1} s^{-1}	expanded *M*-plot[e] $10^{-8}k_{12}$, M^{-1} s^{-1}
9.12	20.0	2.3[f]	4.3	−2.05 ± 0.02	3×10^{-25}	5.7 ± 0.8	0.92 ± 0.04
3.10	17.5	2.5	4.5	7.6 ± 0.4	2×10^{-33}	1.74 ± 0.01	1.04 ± 0.08
3.10	14.0	2.5	5.7	2.5 ± 0.2	1×10^{-25}	1.22 ± 0.06	0.92 ± 0.03
3.10	10.5	2.5	7.8	1.8 ± 0.1	1×10^{-17}	1.27 ± 0.05	1.02 ± 0.04
4.38	10.7	2.1[g]	7.9	3.27 ± 0.06	4×10^{-15}	2.17 ± 0.03	0.90 ± 0.03
3.10	7.01	2.5	12	1.40 ± 0.01	9×10^{-10}	1.15 ± 0.04	0.98 ± 0.05
2.32	5.20	1.9	17	1.42 ± 0.05	2×10^{-7}	1.24 ± 0.02	0.86 ± 0.02
1.58	3.56	1.3	24	1.10 ± 0.01	2×10^{-5}	1.01 ± 0.03	0.92 ± 0.04
3.10	3.51	2.5	29	0.98 ± 0.03	0.15	NA[h]	NA
0.771	2.00	0.62	42	0.998 ± 0.005	0.001	0.979 ± 0.006	0.87 ± 0.02
0.792	1.78	0.65	48	0.86 ± 0.01	0.007	0.845 ± 0.002	0.80 ± 0.01
0.367	1.48	0.29	54	0.98 ± 0.02	0.04	0.98 ± 0.02	0.84 ± 0.02
1.58	1.78	1.3	57	0.87 ± 0.03	0.32	NA	NA
0.367	1.11	0.29	75	0.953 ± 0.005	0.004	0.96 ± 0.01	0.95 ± 0.05
0.792	0.889	0.65	115	0.81 ± 0.01	0.52	NA	NA
0.367	0.738	0.29	118	0.90 ± 0.03	0.048	1.01 ± 0.04	1.07 ± 0.05

[a] Conditions: Full velocity range (12.5–3 m s^{-1}), 0.5 M H_2SO_4, λ_{obsd} = 487 nm, and T = 25.0 ± 0.1 °C. [b] $t_{1/2}$ calculated by eq 12 where k_{12} = (9.28 ± 0.06) × 10^7 M^{-1} s^{-1} for the calibration reaction given in eq 16. [c] k_{12} calculated by eq 15. [d] k_{12} calculated by eq 18. [e] k_{12} calculated by eq 19. [f] λ_{obsd} = 520 nm. [g] λ_{obsd} = 500 nm. [h] NA: not available because $qe^{-R} > 0.05$.

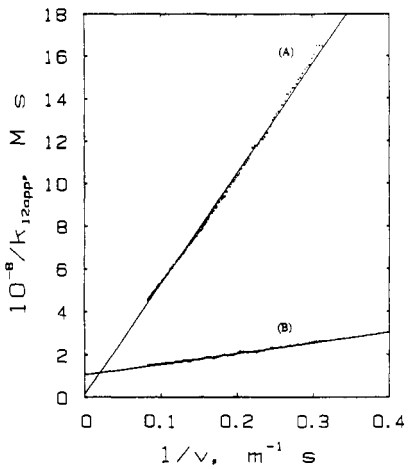

Figure 2. Double-reciprocal plots for the reaction of $W(CN)_8^{4-}$ + $IrCl_6^{2-}$ under second-order, unequal concentration conditions: A, initial $t_{1/2}$ = 4.5 μs; B, initial $t_{1/2}$ = 75 μs. The plots are least-squares lines, weighted in proportion to velocity. The reciprocal of the intercept gives the second-order rate constants of 7.6 ± 0.4 × 10^8 M^{-1} s^{-1} for A and 0.98 ± 0.02 × 10^8 M^{-1} s^{-1} for B.

precision is not as high as that for the first-order *M*-plot ($(A_v - A_\infty)/(A_0 - A_\infty)$ vs v) method which does not require iteration and yields a rate constant from the reciprocal of the slope. Figure 2 is the second-order double-reciprocal analysis for the reaction conditions of $[IrCl_6^{2-}]$ = 3.10 × 10^{-4} M, $[W(CN)_8^{4-}]$ = 1.75 × 10^{-3} M, and $(t_{1/2})_i$ = 4.5 μs for line A, whereas $[IrCl_6^{2-}]$ = 3.67 × 10^{-5} M, $[W(CN)_8^{4-}]$ = 1.11 × 10^{-4} M, and $(t_{1/2})_i$ = 75 μs for line B. Although both double reciprocal plots appear to be resonable linear fits and plot B gives k_{12} = (9.5 ± 0.1) × 10^7 M^{-1} s^{-1}, as expected, plot A gives a k_{12} value of (7.6 ± 0.4) × 10^8 M^{-1} s^{-1}, which is 720% too large.

We know from previous studies[18,24] of first-order reactions that deviations from linearity occur in *M*-plots when conditions give $t_{1/2}$ values less than 10 μs. These deviations have been attributed to different mixing behavior in the center of the twin-path cell. Since integrated observation is used, these deviations are observed only when a significant fraction of the reaction takes place near the cell center. Iteration procedures used for the double reciprocal plots appear to mask these deviations.

If $qe^{-R} \ll 1$, the iteration on R (eq 14) can be eliminated. This condition occurs when C_A is relatively large, when there is a significant excess of one reactant over the other, and/or when k_{12app} (eq 15) is large. Values of R are calculated from the average k_{12app} (6 × 10^7 M^{-1} s^{-1}) from the calibration data and a value of 12 m s^{-1} for the velocity, since it is the worst case condition. The data in Table III show that qe^{-R} becomes very small for $(t_{1/2})_i$ values below 25 μs, where the double-reciprocal plots give the greatest error in the measured rate constant. If q^{-R} is less than 0.05, this term can be neglected and eq 14 can be written as shown by eq 17. Since $qe^{-R} \ll 1$, k_{12app} can be solved directly

$$M_{exptl} = \frac{A_v - A_A(1-q) - A_P}{A_A + (1/q)(A_B - A_P)} = \frac{v}{bk_{12app}C_A} \ln \frac{1}{1-q} \quad (17)$$

by eq 17 without the need for iteration. Substitution of eq 15 for k_{12app} in eq 17 gives eq 18 where a plot of M_{exptl} versus v has a

$$M_{exptl} = \left(\frac{1}{k_{m12}} + \frac{v}{k_{12}}\right) \frac{\ln[(1-q)^{-1}]}{C_A b} \quad (18)$$

slope that is inversely proportional to k_{12} and an intercept that is inversely proportional to k_{m12}. (Equation 18 is referred to as a second-order *M*-plot.) Table III compares the change in the experimental rate constants for the different analysis methods. A second-order *M*-plot analysis for $(t_{1/2})_i$ = 75 μs corresponding to the data from Figure 2B is given in Figure 3. The experimental rate constant is 9.6 × 10^7 M^{-1} s^{-1}, which agrees with the value from the double-reciprocal plot. The rate constants from the second-order *M*-plots for $(t_{1/2})_i$ values below 25 μs deviate less from the expected k_{12} value than in the double-reciprocal evaluation. However, the values are still as much as 88% too large for $[IrCl_6^{2-}]$ = 3.10 × 10^{-4} M, $[W(CN)_8^{4-}]$ = 1.75 × 10^{-3} M, and $(t_{1/2})_i$ = 4.5 μs, where the experimental rate constant is 1.74 × 10^8 M^{-1} s^{-1}.

As in the pseudo-first-order case, a third term[18,24] is added to account for the mixing behavior at the center of the twin-path cell for fast reactions so that eq 18 is modified to give an expanded second-order *M*-plot (eq 19).

$$M_{exptl} = \left(\frac{1}{k_{m12}} + \frac{v}{k_{12}}\right) \frac{\ln[(1-q)^{-1}]}{C_A b} + \frac{c}{v} \quad (19)$$

Regression of M_{exptl} values on v for eq 19 gives the best fit for k_{12}, k_{m12}, and c. Figure 4 shows data from Figure 2A, where an expanded second-order *M*-plot is used. The curvature due to the c/v term is fit by the expanded second-order *M*-plot. The experimental rate constants obtained from the expanded second-order *M*-plot now agree with the predicted rate constant to within

(24) Troy, R. C.; Kelley, M. D.; Nagy, J. C.; Margerum, D. W. *Inorg. Chem.* **1991**, *30*, 4838–4845.

Table IV. Values of k_{12}, k_m, and c (Eqs 19 and 20) from the Different Second-Order Analysis Methods[a]

$10^4[IrCl_6^{2-}]$, M	$10^4[W(CN)_8^{4-}]$, M	$t_{1/2}$, μs	second-order method	$10^{-8}k_{12}$, M^{-1} s^{-1}	$10^{-3}k_m$, m^{-1}	10^3c
9.12	20.0	4.3	expanded M-plot	0.92	3.8	16
3.10	17.5	4.5	expanded *M*-plot	1.04	4.2	3.1
3.10	14.0	5.7	expanded *M*-plot	0.92	4.3	4.3
3.10	10.5	7.8	expanded *M*-plot	1.02	4.1	4.8
4.38	10.7	7.9	expanded *M*-plot	0.90	3.7	13
3.10	7.01	12	expanded *M*-plot	0.98	4.2	7.5
2.32	5.20	17	expanded *M*-plot	0.86	3.7	17
1.58	3.56	24	*M*-plot	1.01	3.8	NA
3.10	3.51	29	double reciprocal	0.98	3.3	NA
0.771	2.00	42	*M*-plot	0.979	2.5	NA
0.792	1.78	48	*M*-plot	0.845	3.2	NA
0.367	1.48	54	*M*-plot	0.98	2.1	NA
1.58	1.78	57	double reciprocal	0.87	2.8	NA
0.367	1.11	75	*M*-plot	0.96	2.2	NA
0.792	0.889	115	double reciprocal	0.81	2.3	NA
0.367	0.738	118	*M*-plot	1.01	2.1	NA

[a] Conditions: Full velocity range (12.5–3 m s^{-1}), 0.5 M H_2SO_4, and T = 25.0 ± 0.1 °C.

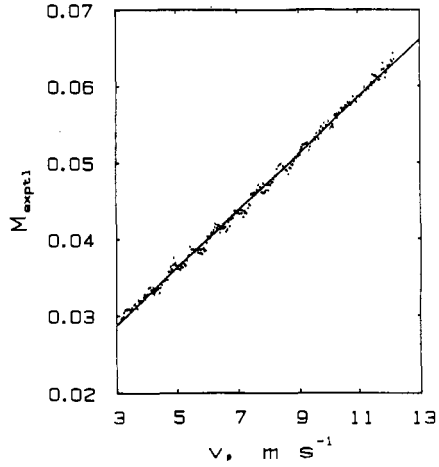

Figure 3. Plot of M_{expt} $((A_o - A_A(1-q) - A_P)/(A_A + (1/q)(A_B - A_P))$ versus velocity for a fast reaction analyzed by the second-order *M*-plot: 1.11×10^{-4} M $W(CN)_8^{4-}$ and 0.367×10^{-4} M $IrCl_6^{2-}$ in H_2SO_4, where $k_r = 0.98 \pm 0.01 \times 10^8$ M^{-1} s^{-1} and initial $t_{1/2}$ = 75 μs.

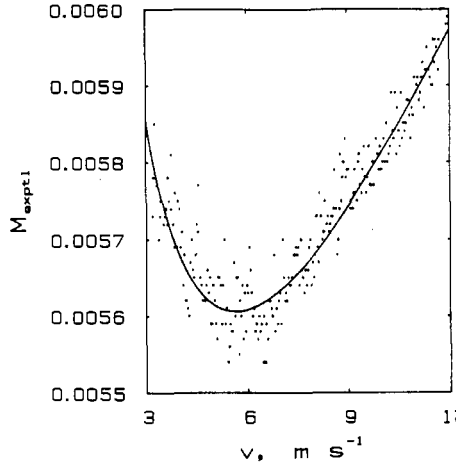

Figure 4. Plot of M_{expt} $((A_o - A_A(1-q) - A_P)/(A_A + (1/q)(A_B - A_P))$ versus velocity for a fast reaction analyzed by the expanded-second-order *M*-plot: 1.75×10^{-4} M $W(CN)_8^{4-}$ and 3.10×10^{-4} M $IrCl_6^{2-}$ in H_2SO_4, where $k_r = 1.04 \pm 0.06 \times 10^8$ M^{-1} s^{-1} and initial $t_{1/2}$ = 4.5 μs.

±10%. The c/v term is needed only for reactions with initial half-lives less than 25 μs.

Table IV contains the calibration data with the rate constants from the proper analysis method and the corresponding mixing constant, k_m (m^{-1}). The average value of the rate constant from the calibration data is $(9.4 \pm 0.7) \times 10^7$ M^{-1} s^{-1}. The mixing constant under second-order concentration conditions (k_{m12}, M^{-1} m^{-1}) decreases with increasing initial concentration. A mixing constant independent of changes in concentration can be calculated from eq 20, The average value of k_m is $(3.3 \pm 0.8) \times 10^3$ m^{-1}

$$k_m = k_{m12}C_A \tag{20}$$

from Table IV, which is in good agreement with the average value of k_m of $(4 \pm 1) \times 10^3$ m^{-1} reported by Nemeth et al.[6]

Kinetics of OBr^- and HOBr Reactions with CN^-. The reactions were run on the PAF-IV under second-order unequal concentration conditions (Table V) with excess hydroxide ion (0.497 and 0.106 M NaOH). The results were analyzed by the expanded second-order *M*-plot method. Variation of the ratio of cyanide to hypobromite from 2:1 to 5:1 gave the same k_{obsd} values of $(5.2 \pm 0.7) \times 10^7$ M^{-1} s^{-1} (eq 21) for seven sets of conditions and

$$-d[OBr^-]/dt = k_{obsd}[OBr^-][CN^-] \tag{21}$$

confirmed the assumed second-order dependence. All trials gave excellent fits for eq 19, and reactions with $(t_{1/2})_i$ as small as 3.1 μs were measured. The mechanism for the reaction of OBr^- and CN^- (eqs 22–24) should be similar to the reaction of OCl^- and

$$OBr^- + CN^- \xrightarrow{k_1} \text{products} \tag{22}$$

$$OBr^- + H_2O \underset{k_{-2}}{\overset{k_2}{\rightleftharpoons}} HOBr + OH^- \tag{23}$$

$$HOBr + CN^- \xrightarrow{k_3} BrCN + OH^- \tag{24}$$

$$\frac{-d[OBr^-]}{dt} = \left(k_1 + \frac{k_2k_3}{k_{-2}[OH^-] + k_3[CN^-]}\right)[OBr^-][CN^-] \tag{25}$$

CN^-.[2] The rate expression in eq 25 results from assuming a steady state in [HOBr] from eqs 22–24. Under the experimental conditions, $[OH^-] \gg [CN^-]$; therefore $k_{-2}[OH^-] \gg k_3[CN^-]$ because $k_{-2} \approx 3 \times 10^9$ M^{-1} s^{-1} (estimated from ΔpK_a values[25]), and k_3 must be less than the diffusion-limited value of 7×10^9 M^{-1} s^{-1}. The second-order observed rate constant, k_{obsd}, is given in eq 26. In order to observe an inverse hydroxide dependence,

$$k_{obsd} = k_1 + \frac{K_w}{K_a^{HOBr}}\frac{k_3}{[OH^-]} \tag{26}$$

the change in the hydroxide concentration must cause a change greater than 10% in the second-order observed rate constant. (It

(25) Eigen, M. *Angew. Chem., Int. Ed. Engl.* **1964**, *3*, 1–72.

Table V. PAF Measurements of Second-Order Rate Constants for the Reactions of Hypobromite and Hypoiodite with Cyanide[a]

$10^3[OX^-]$, M	$10^3[CN^-]$, M	$[OH^-]$, M	$10^{-7}k_{obsd}$, M^{-1} s^{-1}	$(t_{1/2})_i$, μs
		OBr^- Reactions[b]		
0.935	1.89	0.497	6 ± 1	7.1
0.935	2.84	0.497	5.2 ± 0.7	5.2
0.935	3.79	0.497	4.4 ± 0.7	4.5
0.935	4.74	0.497	5.0 ± 0.9	3.1
0.968	1.91	0.106	5.6 ± 0.9	7.6
0.968	2.86	0.106	7 ± 1	3.8
0.968	3.81	0.106	5 ± 1	3.9
0.845	1.55	0.00162	6 ± 2[c]	8.9
0.917	1.55	0.000933	9 ± 1[c]	6.0
0.745	1.55	0.000407	10 ± 4[c]	5.2
		OI^- Reactions[d]		
1.04	2.37	0.965	6 ± 2	5.6

[a] Conditions: 25.0 ± 0.1 °C, μ = 1.00 (with $NaClO_4$/NaOH). [b] λ_{obsd} = 329 nm. [c] $[CO_3^{2-}]_T$ = 0.2 M. [d] λ_{obsd} = 280 nm.

has been determined that k_1 is 5.2×10^7 M^{-1} s^{-1} and $k_2/k_{-2} = 10^{-5}$, where pK_w is 13.79[26] (25 °C, μ = 1.0 M) and pK_a^{HOBr} is 8.59 (25 °C, μ = 1.0 M).) When $[OH^-] > 0.5$ M, as in Table V, $k_1 \gg 10^{-5}k_3/[OH^-]$ even if k_3 were as large as the diffusion-controlled limit. In order to test for an HOBr path, the $[OH^-]$ must be less than 10^{-2} M, and at least a 2-fold variation in $[OH^-]$ is needed. However, under these conditions, the inequality to give k_{obsd} in eq 26 ($k_{-2}[OH^-] \gg k_3[CN^-]$) will not be valid.

To avoid this problem, carbonate buffer was added (eq 27) to keep the $[OH^-]$ low so that the proton transfer in eq 23 would

$$OBr^- + HCO_3^- \underset{k'_{-2}}{\overset{k'_2}{\rightleftharpoons}} HOBr + CO_3^{2-} \qquad (27)$$

not limit the reaction. The new rate expression (eq 28) takes into

$$\frac{-d[OBr^-]'}{dt} = \left(k_1 + \frac{(k_2 + k'_2[HCO_3^-])k_3}{k_{-2}[OH^-] + k'_{-2}[CO_3^{2-}] + k_3[CN^-]}\right) \times [OBr^-][CN^-] \qquad (28)$$

account the role of the carbonate buffer. A total carbonate concentration of 0.2 M was used (Table V). The $p[H^+]$ value was taken after mixing. An inverse hydroxide dependence was expected (eq 29) if $(k_{-2}[OH^-] + k'_{-2}[CO_3^{2-}]) \gg k_3[CN^-]$. A plot

$$k'_{obsd} = k_1 + \frac{K_w}{K_a^{HOBr}}\frac{k_3}{[OH^-]} \qquad (29)$$

of the k'_{obsd} versus $1/[OH^-]$ would be a straight line with a slope proportional to k_3 and an intercept equal to k_1. An inverse hydroxide dependence, as shown in Figure 5, was observed. The lowest hydroxide concentration has a large standard deviation; therefore, a weighted linear regression was used to analyze the data so that the lowest $[OH^-]$ would not bias the analysis. Each second-order rate constant was corrected for the amount of HCN present, where pK_a^{HCN} = 8.95[27] (25 °C, μ = 1.00 M). This correction was insignificant at high hydroxide concentrations but had a small effect in the buffered experiments. The second-order rate constants are $k_1 = (5.7 \pm 0.4) \times 10^7$ M^{-1} s^{-1} and $k_3 = (4.2 \pm 0.9) \times 10^9$ M^{-1} s^{-1}. The standard deviation associated with the HOBr pathway is high but the reaction is extremely rapid.

Kinetics of OI^- and HOI Reactions with CN^-. The disproportionation reactions for OI^- (eqs 30–33)[11] are faster than those of OCl^- and OBr^- under conditions where the hydroxide concentration is less than 0.5 M. In order to stabilize the OI^-,

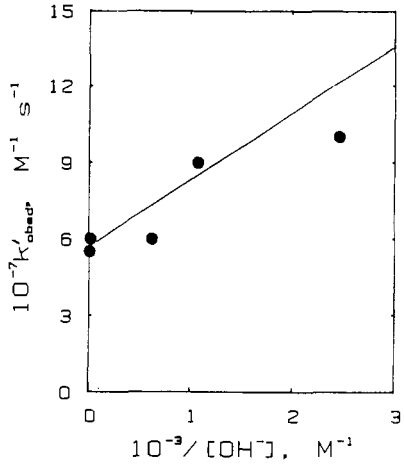

Figure 5. Dependence of the second-order rate constant for the reaction of OBr^- and CN^- on the reciprocal of the OH^- concentration (data from Table V). The line shown is a weighted linear regression.

Table VI. Comparison of Rate Constants of Cyanide with Hypohalites and Hypohalous Acids[a]

halogen	OX^- k_1, M^{-1} s^{-1}	HOX $10^{-9}k_3$, M^{-1} s^{-1}
Cl[b]	310	1.22
Br	5.7×10^7	4.2
I	6×10^7	7[c]

[a] Conditions: 25.0 ± 0.1 °C and μ = 1.00 M (with $NaClO_4$). [b] Reference 2. [c] Predicted value.

$$OI^- + I^- + H_2O \rightleftarrows I_2OH^- + OH^- \quad K = 0.15 \qquad (30)$$

$$OI^- + OI^- \rightarrow IO_2^- + I^- \quad k \le 7.2 \times 10^{-2}\ M^{-1}\ s^{-1} \qquad (31)$$

$$OI^- + HOI \rightarrow IO_2^- + I^- + H^+ \quad k = 40\ M^{-1}\ s^{-1} \qquad (32)$$

$$OI^- + I_2OH^- \rightarrow IO_2^- + 2I^- + H^+ \quad k = 6\ M^{-1}\ s^{-1} \qquad (33)$$

a higher hydroxide concentration is used ($[OH^-] > 0.9$ M). Even under these conditions, the OI^- concentration decreases by a factor of 2 in 90 min. The disappearance of OI^- in its reaction with CN^- is too fast to measure by stopped-flow spectroscopy, so pulsed-accelerated-flow spectroscopy is used. An absorbance shoulder at 280 nm [10] is used as the λ_{obsd} to give an initial absorbance of 0.50 and a final absorbance of 0.09 (ΔA_T = 0.41). The final absorbance at 280 nm is due to I^- present in the solution. The reactant concentrations are $[OI^-] = 1.04 \times 10^{-3}$ M and $[CN^-] = 2.37 \times 10^{-3}$ M (both in 0.965 M NaOH), and the measured rate constant is $(6 \pm 2) \times 10^7$ M^{-1} s^{-1}. The assumption is made that the value of 6×10^7 M^{-1} s^{-1} corresponds to the k_1 path because the conditions were such that the pH was at least 3 log units away from the pK_a of HOI of 10.0 ± 0.3.[11] In order to measure the rate constant for the reaction of hypoiodous acid with cyanide, the $[OH^-]$ concentration must be lowered substantially, and HOI disproportionation reactions make the measurements very difficult. We expect the rate constant for HOI to be larger than the values for either HOCl or HOBr with CN^- (Table VI). This is due to the greater case of I^+-transfer compared to Br^+-transfer or Cl^+-transfer. Iodine can more readily expand its coordination due to the increased availability of empty low-energy orbitals. Since the rate constants for HOCl and HOBr with CN^- are 1.22×10^9 M^{-1} s^{-1} and 4.2×10^9 M^{-1} s^{-1}, respectively, the rate constant for HOI with CN^- may be as large as the diffusion-controlled limit of 7×10^9 M^{-1} s^{-1}.

Identification and Base Hydrolysis of Products. As with hypochlorite, there is ample evidence that the reactions of bromine or iodine with cyanide will give cyanogen bromide[1,3,4] or cyanogen

(26) Smith, R. M.; Martell, A. E. *Critical Stability Constants, Vol. 4: Inorganic Complexes*; Plenum Press: New York, 1976; p 1.
(27) Gübeli, A. O.; Côté, P. A. *Can. J. Chem.* **1972**, *50*, 1144–1148.

Table VII. ^{13}C NMR Chemical Shifts

species	resonance freq, ppm[a]	species	resonance freq, ppm[a]
CN^-	166.3	OCN^-	129.63[b]
BrCN	82.3	CO_3^{2-}	169.4
ICN	50.39		

[a] Referenced to an internal standard of dioxane (67.40 ppm). [b] A triplet at 129.42, 129.63, and 129.85 ppm with intensities of 1:2:1.

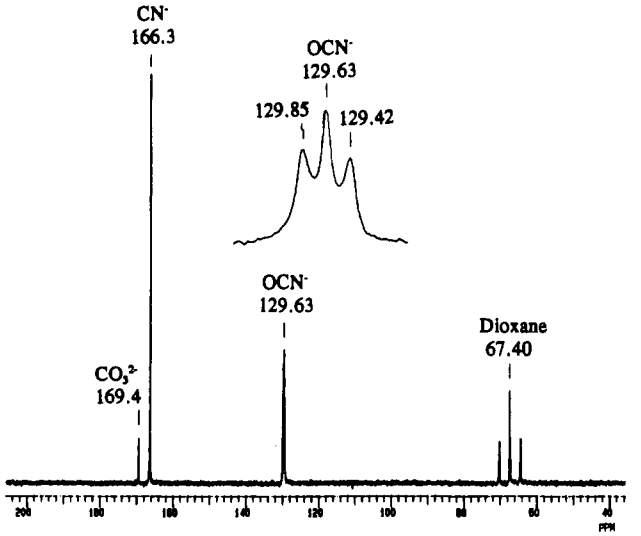

Figure 6. ^{13}C-NMR spectrum of a solution, 12 h after mixing, which initially contained 0.167 M OBr^-, 0.280 M $Na^{13}CN$, and 0.48 M NaOH.

iodide,[1,5] respectively. Williams[1] cites references to several methods of generating BrCN and ICN from the reactions of bromine or iodine with cold aqueous solutions of hydrogen cyanide.

Cyanogen Bromide. We have used ^{13}C NMR to help identify the presence and reactions of cyanogen halides. In high base concentration the reaction between OCl^- and CN^- rapidly gives OCN^- and Cl^- (eq 34) because of the base hydrolysis of ClCN

$$OCl^- + CN^- \rightarrow OCN^- + Cl^- \quad (34)$$

(eq 4). One hour after mixing, the ^{13}C NMR spectrum of a solution initially containing 0.19 M OCl^-, 0.22 M $Na^{13}CN$, and 0.8 M NaOH gives a triplet centered at 129.63 ppm due to OCN^-. This observation agrees well with the resonance frequency for OCN^- at 128.8 ppm reported by Bleasdale et al.[28] and the resonance frequency of 129.7 ppm reported by Maciel and Beatty.[29] Table VII contains a summary of the relevant species and their resonance frequencies.

A solution that contained 0.167 M OBr^-, 0.280 M $Na^{13}CN$, and 0.48 M NaOH after mixing also had a triplet centered at 129.63 ppm in the ^{13}C-NMR spectrum after 12 h (Figure 6). The CN^- in this reaction is converted to OCN^- (eq 35), but this fact

$$OBr^- + CN^- \rightarrow OCN^- + Br^- \quad (35)$$

does not rule out BrCN as an intermediate. Although the splitting from nitrogen ($I = 1$) might be expected to give three peaks of equal height, the OCN^- ^{13}C-NMR peaks in Figure 6 appear to have a splitting pattern of 1:2:1. The reason for the discrepancy is that the T_1 of the N nucleus is extremely short because N is strongly relaxed by its environment.[30] In some cases the lifetime of the second nucleus is so short that the spin–spin splitting disappears completely (such as PBr_5 or $CHCl_3$). The peak at

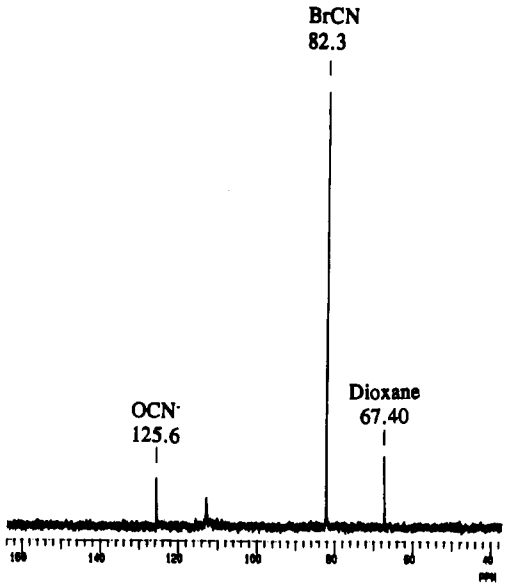

Figure 7. ^{13}C-NMR spectrum of a solution prepared as follows: 1 mL of OBr^- at pH = 10 was added to 0.021 g of $Na^{13}CN$, and immediately after the cyanide was dissolved (5 s), 1 mL of 1 M $HClO_4$ and 1 mL of D_2O were added.

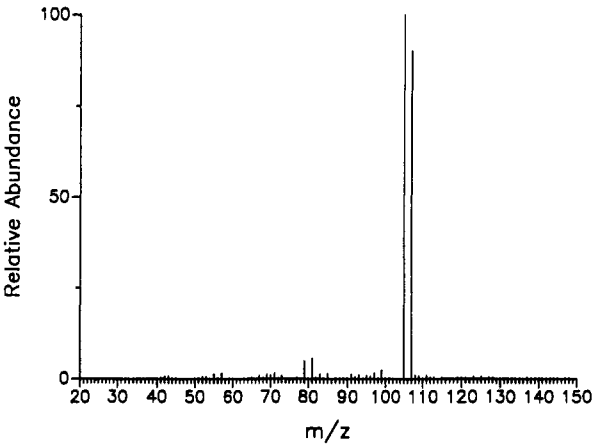

Figure 8. Mass spectrum (MIMS technique) of the products of Br_2 reaction with NaCN at pH = 2.14. Peaks at 105 and 107 amu correspond to $^{79}BrCN$ and $^{81}BrCN$.

67.4 ppm is the internal reference, dioxane. The peak at 166.3 ppm is due to the excess $^{13}CN^-$, which agrees with the value of 167 ppm for KCN in an aqueous solution.[31] Cyanate can hydrolyze in base to give CO_3^{2-} [33a] and NH_3.[32] The small peak at 169.4 ppm is due to CO_3^{2-}.[33a] Figure 7 is the ^{13}C-NMR spectrum of a solution prepared as follows: 1 mL of 0.20 M OBr^- at pH = 10 was added to 0.021 g of $Na^{13}CN$; after the labeled cyanide was dissolved (5 s), 1 mL of 1 M $HClO_4$ and 1 mL of D_2O (for signal lock) were added. The spectrum of this solution contains a peak at 82.3 ppm. This peak is due to BrCN[33b] (a resonance frequency at 77.4 ppm was previously reported[33b] for BrCN in $CDCl_3$ solution). The 82.3 ppm resonance also is observed when Br_2 is mixed with excess $Na^{13}CN$ under acidic conditions. The small peaks at 125.6 and 112 ppm are due to OCN^-/HOCN and the transmitter frequency, respectively. It is difficult to study the base hydrolysis of BrCN by ^{13}C-NMR because it takes approximately 20 min to acquire each ^{13}C-NMR spectrum.

(28) Bleasdale, C.; Golding, B. T.; McGinnis, J.; Muller, S.; Watson, W. P. *J. Chem. Soc., Chem. Commun.* **1991**, 1726–1728.
(29) Maciel, G. E.; Beatty, D. A. *J. Phys. Chem.* **1965**, *69*, 3920–3924.
(30) Carrington, A.; McLachlan, A. *Introduction to Magnetic Resonance with Applications to Chemistry and Chemical Physics*; Harper and Row Publishers: New York, 1979; p 210.
(31) Jones, M. M.; Beaty, J. A. *Inorg. Chem.* **1991**, *30*, 1584–1587.
(32) Lister, N. W. *Can. J. Chem.* **1955**, *33*, 526–540.
(33) *Sadtler Standard Carbon-13 NMR Spectra*; Sadtler Research Laboratories, eds.; Sadtler Research Laboratories, Inc.: Philadelphia, PA: (a) Vols. 151–152, 1991, no. 30003; (b) Vols. 122–123, 1988, no. 24530; (c) Vols. 143–144, 1990, no. 28693.

Table VIII. Observed Rate Constant for the Base Hydrolysis of BrCN[a]

$[OH^-]$, M	$[CO_3^{2-}]_T$, M	k_{obsd}, s^{-1}
0.105	NA	0.0554
0.105	NA	0.0578
0.105	NA	0.0563
0.105	NA	0.0563
0.105	NA	0.0563
0.105	NA	0.0533
0.105	NA	0.0573
1.047×10^{-4}	0.20	0.00087
1.047×10^{-4}	0.30	0.00124
1.047×10^{-4}	0.40	0.00167

[a] Conditions: 25 ● 1 °C, μ = 1.00 (with $NaClO_4$), decrease of 105 amu signal monitored by MIMS.

Membrane introduction mass spectrometry (MIMS)[19] has made it possible to isolate and detect neutral molecules in aqueous solutions. Therefore, MIMS is used in this work to isolate BrCN and study its decomposition in base. BrCN (0.01 M) was prepared by mixing excess NaCN with Br_2 in acid. The solution was diluted 5-fold with water, and the pH was adjusted to 2.14. The mass spectrum of this sample (obtained by use of the MIMS technique) is given in Figure 8. The peaks at 105 and 107 amu are due to $^{79}BrCN$ and $^{81}BrCN$, and there is no evidence of Br_2. The base hydrolysis of BrCN, as given in eq 36, was studied by following

$$BrCN + 2OH^- \rightarrow OCN^- + Br^- + H_2O \qquad (36)$$

its disappearance at 105 amu with MIMS. The experimental rate law is given in eq 37. The value for k_{OH} was determined by

$$-d[BrCN]/dt = (k_{OH}[OH^-] + k_{CO_3}[CO_3^{2-}])[BrCN] \qquad (37)$$

reacting 0.005 M OBr^- with 0.006 M CN^- at $[OH^-]$ = 0.105 M (25 ± 1 °C, μ = 1.00 M). Upon mixing, the sample was introduced into a membrane probe and initial signal detection was in 11 s, while the signal peaked typically in 20 s. The half-life for this reaction was measured as ~12 s, which, considering a dead time of 20 s, is near the limit of half-lives measurable under these conditions with this instrumental design. Table VIII summarizes the OH^- reaction data and conditions. The value of k_{OH} was determined as 0.53 ± 0.01 M^{-1} s^{-1}.

The value for k_{CO_3} was determined by reacting 0.005 M BrCN at pH 2 with carbonate buffer solutions where $[CO_3^{2-}]_T$ varied from 0.4 to 0.8 M (25 ± 1 °C, μ = 1.00 M). The final pH of these mixtures was 9.62. A sample mass chromatogram is shown in Figure 9. To evaluate k_{CO_3}, eq 38 is derived from eq 37 in

$$\frac{k_{obsd}}{[OH^-]} = k_{OH} + k_{CO_3}\frac{[CO_3^{2-}]_T}{[OH^-] + K_{CO_3}} \qquad (38)$$

terms of $[CO_3^{2-}]_T$. A plot of $k_{obsd}/[OH^-]$ vs $[CO_3^{2-}]_T/([OH^-] + K_{CO_3})$, where $K_{CO_3} = 10^{-4}$, is given in Figure 10, and data for the MIMS experiment are included in Table VIII. The slope of the line gives $k_{CO_3} = (7.5 \pm 0.1) \times 10^{-3}$ M^{-1} s^{-1}. The intercept gives $k_{OH} = 0.54 \pm 0.15$ M^{-1} s^{-1}. This k_{OH} value agrees with the value obtained in the excess hydroxide experiment.

Bailey and Bishop[34] studied the base hydrolysis of ClCN and determined a rate law similar to eq 37. Their rate constants were 4.53 M^{-1} s^{-1} for k_{OH} and 3.3×10^{-2} M^{-1} s^{-1} for k_{CO_3}.

Cyanogen Iodide. ^{13}C-NMR spectra were used to confirm that the reactant is ICN[33c] and the final product is OCN^-. A saturated solution of ICN in water has a resonance frequency of 50.39 ppm (Table VII). This value agrees well with the reported value of 49.2 ppm.[33c] Diluting ICN in base produced a triplet centered at 129.63 ppm due to the formation of $O^{13}CN^-$.

(34) Bailey, P. L.; Bishop, E. *J. Chem. Soc., Dalton Trans.* **1973**, *9*, 912–916.

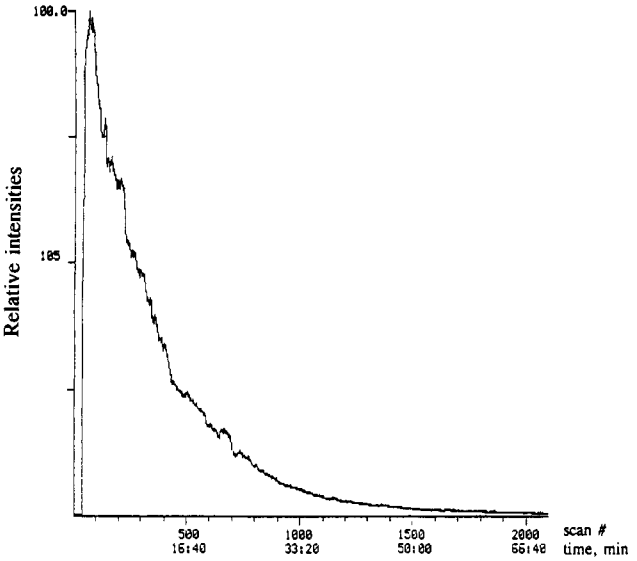

Figure 9. Mass chromatogram of the base hydrolysis of BrCN (p[H^+] = 9.62 and $[CO_3^{2-}]_T$ = 0.3 M) at 105 amu. The rate constant is 1.24×10^{-3} s^{-1}.

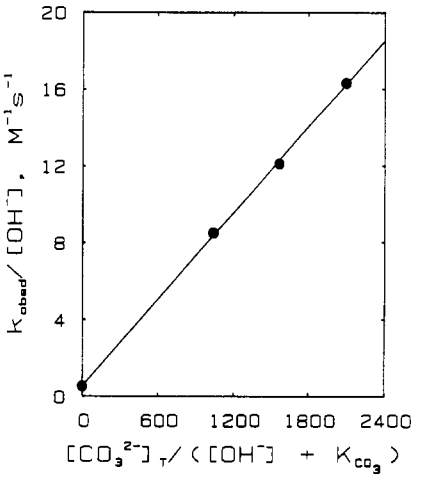

Figure 10. Plot of $k_{obsd}/[OH^-]$ versus $[CO_3^{2-}]_T/([OH^-] + K_{CO_3})$ for the carbonate buffer dependence of the base hydrolysis of BrCN. The slope is k_{CO_3} ((7.5 ● 0.1) × 10^{-3} M^{-1} s^{-1}) and the intercept is k_{OH} (0.54 ± 0.15 M^{-1} s^{-1}).

Table IX. Observed Rate Constants for the Base Hydrolysis of ICN[a]

$[OH^-]$, M	$10^3 k_{r1}$, s^{-1} [b]	$10^5 k_{r2}$, s^{-1} [b]
0.00492	0.100 ± 0.003	1.8 ± 0.6
0.0582	0.655 ± 0.002	0.21 ± 0.05
0.106	1.00 ± 0.001	NA
0.116	1.14 ± 0.001	0.3 ± 0.5
0.116	1.08 ± 0.01	1.0 ± 0.4
0.272	1.99 ± 0.01	9.0 ± 0.6
0.489	2.63 ± 0.01	1.0 ± 0.9
0.909	3.05 ± 0.02	11 ± 1

[a] Conditions: 25.0 ± 0.1 °C, μ = 1.00 (with $NaClO_4$), I^- released monitored at 225 nm. [b] Errors for the k_r values are the standard deviations given in the FitAll analysis.

The base hydrolysis of cyanogen iodide was monitored spectrophotometrically by the appearance of iodide ion at 225 nm (eq 11). The pseudo-first-order rate constants (Table IX) begin to level off with high $[OH^-]$. The mechanism in Scheme I is proposed to explain this saturation effect. A rapid OH^- association at the iodine atom can be treated as a pre-equilibrium step that produces $HOICN^-$, a species that inhibits the formation of products. Attack of OH^- at the carbon is the rate-determining step to give OCN^- as the final product. Wang et al.[35] and Troy et al.[24] have proposed molecular complexes of ICl and of IBr with

Scheme I

$$HOICN^- \overset{K_{OH}^{-1}}{\rightleftarrows} ICN + OH^- \overset{k_4}{\rightarrow}$$

$$HOCN + I^- \overset{\text{rapid, } +OH^-}{\rightarrow} OCN^- + H_2O + I^-$$

H_2O, OH^-, and buffers. We propose that ICN forms a similar complex ion with hydroxide. Cyanogen iodide is known to form complexes with iodide ion and cyanide ion (eqs 39 and 40).[36] The

$$ICN + CN^- \rightleftarrows I(CN)_2^- \quad K = 2.50\ M^{-1} \qquad (39)$$

$$ICN + I^- \rightleftarrows I_2CN^- \quad K = 1.17\ M^{-1} \qquad (40)$$

concentrations of these complex ions are negligible under our conditions (a maximum of 0.01% I_2CN^- and 2.3% $I(CN)_2^-$). The rate expression is given in eq 41, where $[ICN]_T = [ICN] +$

$$\frac{d[I^-]}{dt} = \frac{k_4[OH^-]}{1 + K_{OH}[OH^-]}[ICN]_T \qquad (41)$$

$[HOICN^-]$. Figure 11 shows a simplex optimization fit of the data in Table IX. K_{OH} is 3.2 ± 0.2 M^{-1} and k_4 is (1.34 ± 0.05) × 10^{-2} M^{-1} s^{-1}. There are actually two pseudo-first-order reactions observed (eq 42). The sum of two first-order exponentials (eq

$$d[I^-]/dt = k_{r1}[ICN]_T + k_{r2}[IO_2^-] \qquad (42)$$

$$A = A_\infty + \Delta A_{r1} \exp(-k_{r1}t) + \Delta A_{r2} \exp(-k_{r2}t) \qquad (43)$$

43) was used to fit the absorbance vs time data, where A_∞ is the absorbance at infinity, ΔA_{r1} is the change in absorbance due to the base hydrolysis of ICN, k_{r1} is the rate constant for the base hydrolysis of ICN, t is time (s), ΔA_{r2} is the change in absorbance due to a slower reaction, and k_{r2} is the smaller rate constant. The second pseudo-first-order reaction, k_{r2}, is attributed to a side reaction of initial reactants. We believe the side reaction results from the presence of iodite formed from the disproportionation of hypoiodite (eq 31).[11] The subsequent reaction of iodite with iodide gives hypoiodite that reacts again with cyanide in eqs 44–46. The overall reaction is given in eq 47. Rate constants for

$$IO_2^- + I^- \overset{k_{r2}}{\rightarrow} 2OI^- \quad \text{(slow)} \qquad (44)$$

$$2OI^- + 2CN^- + 2H_2O \overset{\text{rapid}}{\rightarrow} 2ICN + 4OH^- \qquad (45)$$

$$2ICN + 4OH^- \overset{\text{rapid}}{\rightarrow} 2I^- + 2OCN^- + 2H_2O \qquad (46)$$

$$IO_2^- + 2CN^- \rightarrow I^- + 2OCN^- \qquad (47)$$

the reaction of I^- with IO_2^- in the absence of OI^- have not been determined. In aged solutions of OI^-, there is an appreciable amount of IO_2^- present. When cyanide is added to these solutions, it reacts with OI^- and only the products of the disproportionation of the OI^- remain. A mixture of CN^- and IO_3^- was tested and failed to give any I^- release. Table IX lists the k_{r2} for the different hydroxide concentrations. The contribution from the IO_2^- path is small under our conditions.

To confirm that the faster reaction was due to the hydrolysis of ICN, solid ICN was used to determine the pseudo-first-order rate constant in 0.106 M NaOH. The observed rate constant was 1.00 × 10^{-3} s^{-1} compared to the calculated rate constant of (1.08 ± 0.04) × 10^{-3} M^{-1} s^{-1} from eq 39, with the uncertainty estimated from propagation of errors. Therefore, we are confident that the larger pseudo-first-order rate constant, k_{r1}, is due to the hydrolysis of ICN.

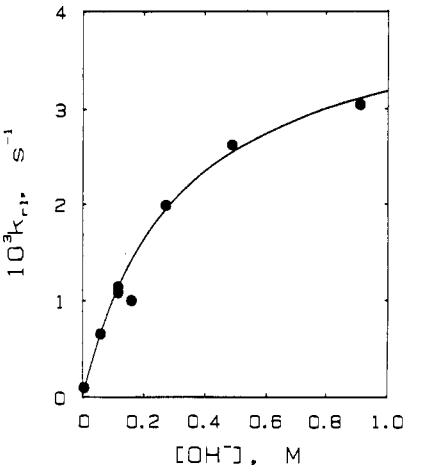

Figure 11. Dependence of the first-order rate constant on $[OH^-]$ for the base hydrolysis of ICN.

Table X. Comparison of Rate Constants for the Base Hydrolysis of Cyanogen Halides[a]

cyanogen halide	rate consts, M^{-1} s^{-1}	
	$[OH^-]$	$[CO_3^{2-}]$
ClCN	4.53[b]	3.3 × 10^{-2} [b]
BrCN	0.53	7.5 × 10^{-3}
ICN	0.0134	

[a] Conditions: 25.0 °C, μ = 1.00 M (with $NaClO_4$). [b] Reference 34.

The reaction of OI^- and CN^- may give ICN (eq 48) or might directly give OCN^- (eq 49). A stopped-flow experiment measured

$$OI^- + CN^- + H_2O \rightarrow ICN + 2OH^- \qquad (48)$$

$$OI^- + CN^- \rightarrow OCN^- + I^- \qquad (49)$$

the initial amount of I^- released from the reaction of OI^- and CN^- in high OH^- concentrations, where the amount of HOI is small (pK_a = 10.0 ± 0.3).[11] This was done in order to establish whether the reaction of OI^- with CN^- gives ICN or OCN^-. If k_1 is 6 × 10^7 M^{-1} s^{-1} for the OI^- reactions with CN^- and k_3 is equal to or less than 7 × 10^9 M^{-1} s^{-1} for HOI and CN^-, then in 0.88 M NaOH more than 98% of the reaction must be due to the k_1 path. $(t_{1/2})_i$ for the OI^- and CN^- reactions is 11.9 μs, and $t_{1/2}$ for the base hydrolysis of ICN is 224 s. In the first 0.25 s of the reaction there is no increase in the I^- absorbance at 225 nm. Therefore, there is no evidence for oxygen-atom transfer (eq 49), and the reaction product even at high base is due to I^+-transfer (eq 48). If the reaction had proceeded by oxygen-atom transfer, the initial release of I^- in 0.25 s would increase the absorbance by 0.0959. We predict from this evidence that the reactions of hypochlorite and hypobromite (k_1 path) with cyanide also take place via a halogen-cation transfer, to give ClCN and BrCN, respectively, as initial products.

Conclusion

The OBr^- and OI^- reactions with CN^- are faster than the reaction of OCl^- with CN^-. We propose that the enhanced rates are associated with the greater ease of the I^+-transfer or Br^+-transfer compared to the Cl^+-transfer reaction: nucleophilic attack at iodine and bromine, with their greater ease of expansion of coordination due to their readily available low-energy orbitals,

(35) Wang, Y. L.; Nagy, J. C.; Margerum, D. W. *J. Am. Chem. Soc.* **1989**, *111*, 7838–7844.
(36) Yost, D. M.; Stone, W. E. *J. Am. Chem. Soc.* **1933**, *55*, 1889–1895.

is more favorable than the corresponding attack at chlorine. The relative rates of reactivity for hypohalite reactions with CN^- are $OI^- \approx OBr^- \gg OCl^-$ (Table VI). The reactivity of HOBr is greater than that of OBr^- (by a factor of 73 for CN^-). The HOBr reaction with CN^- is so fast that the rate constant is within a factor of 2 of the diffusion limit. The relative rates of reactivity for the reaction of hypohalous acids with CN^- are HOBr > HOCl.

The rate constants for base hydrolysis of BrCN and ICN are determined. The relative rate constants for the cyanogen halides are in the order ClCN ≫ BrCN ≫ ICN (Table X). The order can be attributed to the relative preference of the leaving groups $Cl^- > Br^- > I^-$.

Acknowledgment. This work was supported by National Science Foundation Grant CHE-9024291. We are grateful to Lindy E. Dejarme and R. Graham Cooks for their assistance in the MIMS experiments and to H. D. Lee for synthesis of $K_4W(CN)_8$. M.G. also thanks The Procter and Gamble Co. for a fellowship.